Operational Analysis of Electric Power Management and Control for a Quadrotor UAV

Yuze Li
Mechanical Engineering Dept.
University College London
London, UK
yuze.li.22@ucl.ac.uk

Pedram Asef
Mechanical Engineering Dept.
University College London
London, UK
pedram.asef@ucl.ac.uk

Pouria Sarhadi
School of Phys., Eng., & Comp. Sci.
University of Hertfordshire
Hatfield, UK
p.sarhadi.@herts.ac.uk

***Abstract*— This study presents the development of an operational analysis framework for the electric propulsion and control systems of quadrotor unmanned aerial vehicles (UAVs) designed for short-range transport missions. A comprehensive 6-DOF dynamics model is developed to enhance simulation realism by incorporating key system characteristics. A three-loop cascade controller architecture is implemented, integrating PID-based position control, MPC-based attitude control for improved responsiveness and disturbance rejection, and precise motor control for real-time voltage and speed regulation. Furthermore, motor and battery configurations are optimized through simulation to meet specific payload requirements. Simulation results verify the system's capability for accurate trajectory tracking, stable flight, and efficient propulsion, providing valuable insights for UAV design and deployment. The proposed framework can also be utilized for power and energy management analysis in the design of electric UAVs.**

Keywords—Electric Propulsion System, Electric Machine, Model Predictive Control, PID Controller, UAV.

NOMENCLATURE

Symbol	Description	Unit
$\dot{V}^B$	Linear acceleration of the quadrotor in B-frame	$m\ s^{-2}$
$\dot{\omega}^B$	Angular acceleration in B-frame	$rad\ s^{-1}$
F^B	Force vector acting on the quadrotor	N
τ^B	Torque vector acting on the quadrotor	N m
Ω	Propeller's speed vector	$rad\ s^{-1}$
U_1	Total thrust generated by all four rotors	N
$[U_2\ U_3\ U_4]$	Control torques for roll, pitch, and yaw	N m
Δt	Controller sampling time	s
N_P	Prediction horizon	-
N_C	Control horizon	-
K_E	Back-EMF constant	$V\ s\ rad^{-1}$
K_M	Motor torque constant	$N\ m\ A^{-1}$
η	Gearbox conversion efficiency	-
N	Gearbox reduction ratio	-
R	Motor resistance	Ω

I. INTRODUCTION

Unmanned aerial vehicles (UAVs) are increasingly used across logistics, agriculture, environmental monitoring, and defense due to their mobility, efficiency, and versatility. While fuel-powered UAVs offer long endurance and high payload capacity, they suffer from noise, pollution, and high maintenance costs. In contrast, electric propulsion systems provide cleaner, quieter, and more efficient alternatives, aligning with sustainability goals [1-2]. However, challenges such as limited flight time, battery constraints, and complex control requirements remain [3]. Addressing these issues through efficient propulsion design and robust control strategies is critical for advancing electric UAV technology. Electric propulsion offers clear advantages over fuel-based systems in higher efficiency, noise reduction, lower cost, and environmental impact, making it ideal for UAVs operating in urban, remote or sensitive areas [1]. Despite these benefits, UAVs face challenges, such as limited flight time due to battery constraints (limited battery energy density) and complex control requirements [4-6].

Among all quadrotors, which are underactuated and inherently unstable, capable control systems are required to manage nonlinear dynamics, payload variations, and external disturbances. The quadrotor is an underactuated, coupled system with six degrees of freedom (DOF) but only four independent control inputs. Without active stabilization, it cannot maintain hover or track a desired state and quickly becomes unstable [7]. UAV dynamics are highly nonlinear and affected by parameter uncertainty and coupling, all of which can reduce control performance. For instance, changes in the payload or aerodynamic drag of a quadrotor can alter its inertia and required thrust, causing model mismatches. These issues highlight the need for highly reliable control architectures [8]. A common UAV control strategy is the PID-based cascade structure, where the inner loop stabilizes attitude, and the outer loop manages position. This approach is simple and effective for near-linear flight conditions. However, its performance degrades during aggressive maneuvers due to nonlinear dynamics, actuator limits, and cross-coupling effects. PID controllers also lack constraint handling and often require retuning across different flight regimes, prompting the exploration of more advanced control methods [9].

To overcome these limitations, the researchers used an approach called Model Predictive Control (MPC). MPC addresses the limitations of PID by predicting system behavior and optimizing control actions in real time, while naturally handling multivariable dynamics and constraints. Though effective in managing UAV coupling and input limits, MPC is computationally intensive, posing challenges for onboard implementation. To balance

performance and efficiency, this study adopts a hybrid approach, using MPC for fast attitude control and PID for slower position control, reducing computational load while maintaining robust flight performance [10].

Crucially, most existing control studies focus primarily on UAV motion, such as position and attitude, with limited integration of motor dynamics and control within the feedback loop. This study addresses that gap by incorporating closed loop electric motor control, motor sizing, and battery performance modeling. It targets short range transport using a mid-weight quadrotor electric UAV, and proposes an innovative electric propulsion system design. A six DOF dynamics model is developed using the Newton Euler method with coordinate transformations to accurately characterize flight behavior. To handle fast response requirements, dynamic coupling, and load disturbances, a hybrid three loop control structure is introduced, combining PID based position control with MPC based attitude control. Also, motor and battery parameters are optimized through simulation to ensure performance under varying payloads.

II. Analytical Analysis

A. Quadrotor Setup

The UAV used in this research is a mid-weight electric quadrotor designed for short-range delivery tasks, with a symmetrical cross-shaped ('+' plus-shaped) structure. The key physical parameters of the quadrotor used in modelling and simulation are summarized in Table I, with reference to the parameters of the DJI AGRAS T40 [12].

TABLE I. Physical Parameters of the Quadrotor

Symbol	Description	Value [unit]
m_{quad}	Mass of the quadrotor	50 [kg]
m	Total mass of the quadrotor and load	50_{min}~100_{max} [kg]
l	Arm length of the quadrotor	1.092 [m]
r_{prop}	Radius of the propeller	0.686 [m]
b	Thrust factor	8.985×10^{-2} [N m s^2]
d	Drag factor	1.668×10^{-3} [N s^2]
J_{TP}	Rotational moment of inertia around the propeller axis	3.551×10^{-2} [kg m^2]
I_{XX}	Moment of inertia along B-frame X-axis	13.507 [kg m^2]
I_{YY}	Moment of inertia along B-frame Y-axis	13.507 [kg m^2]
I_{ZZ}	Moment of inertia along B-frame Z-axis	21.855 [kg m^2]

The quadrotor has six DOF but only four control inputs, making it an underactuated system. Position and attitude control are achieved by adjusting the rotational speeds of the four rotors. To balance the torque generated by each rotor, two spin clockwise and two counterclockwise, producing opposing torques that stabilize the UAV, as illustrated in Fig. 1.

To accurately describe the flight state of the UAV, two reference coordinate frames need to be introduced into the modeling: the Earth inertial frame (E-frame) and the body-fixed frame (B-frame). The orange axes represent the Earth's inertial frame, which is usually fixed to the ground, and the blue axes represent the body-fixed frame, which varies with the movement of the UAV.

B. Kinematic and Dynamic Modeling

The kinematics of a generic 6-DOF rigid body is [13]:

$$\dot{\xi} = J_\Theta \nu \tag{1}$$

The generalized position vector ξ consists of the quadrotor linear Γ^E $[m]$ and angular Θ^E $[rad]$ position vectors for the E-frame. Similarly, the generalized velocity vector ν consists of the quadrotor linear V^B $[m\,s^{-1}]$ and angular ω^B $[rad\,s^{-1}]$ velocity vectors concerning the B-frame, as:

$$\xi = [\Gamma^E \quad \Theta^E]^T = [X \quad Y \quad Z \quad \phi \quad \theta \quad \psi]^T \tag{2}$$

$$\nu = [V^B \quad \omega^B]^T = [u \quad v \quad w \quad p \quad q \quad r]^T \tag{3}$$

The generalized matrix $J_\Theta \in \mathbb{R}^{6\times6}$ acts to map the velocity of the B-frame to the derivatives of the E-frame, which contains a rotation matrix $R_\Theta \in \mathbb{R}^{3\times3}$ and a transfer matrix $T_\Theta \in \mathbb{R}^{3\times3}$.

$$J_\Theta = \begin{bmatrix} R_\Theta & 0_{3\times3} \\ 0_{3\times3} & T_\Theta \end{bmatrix} \tag{4}$$

With the definition of the generalized matrix J_Θ, the linear and angular velocities in the B-frame can be transformed into the corresponding derivatives in the E-frame, see Eqs. (5) and (6).

$$\begin{bmatrix} \dot{X} \\ \dot{Y} \\ \dot{Z} \end{bmatrix} = \begin{bmatrix} c_\theta c_\psi & s_\theta c_\psi s_\phi - s_\psi c_\phi & s_\theta c_\psi c_\phi + s_\psi s_\phi \\ c_\theta s_\psi & s_\theta s_\psi s_\phi + c_\psi c_\phi & s_\theta s_\psi c_\phi - c_\psi s_\phi \\ -s_\theta & c_\theta s_\phi & c_\theta c_\phi \end{bmatrix} \begin{bmatrix} u \\ v \\ w \end{bmatrix} \tag{5}$$

$$\begin{bmatrix} \dot{\phi} \\ \dot{\theta} \\ \dot{\psi} \end{bmatrix} = \begin{bmatrix} 1 & \tan\theta \sin\phi & \tan\theta \cos\phi \\ 0 & \cos\phi & -\sin\phi \\ 0 & \sec\theta \sin\phi & \sec\theta \cos\phi \end{bmatrix} \begin{bmatrix} p \\ q \\ r \end{bmatrix} \tag{6}$$

where the shorthand notations c_x and s_x denote $\cos(x)$ and $\sin(x)$, and x corresponds to the Euler angles roll (ϕ), pitch (θ), yaw (ψ). To fully capture the quadrotor's flight behavior, dynamic equations accounting for external forces and moments are introduced alongside the kinematic model.

This study adopts the Newton-Euler formalism, based on two standard assumptions: 1) The origin of the B-frame (o_B) coincides with the centre of mass; 2) The axes of the B-frame are oriented in the same direction as the principal inertia axis so that the inertia matrix I is a diagonal matrix (13). Thus, the dynamic equation of the quadrotor can be:

$$\begin{bmatrix} m\,I_{3\times3} & 0_{3\times3} \\ 0_{3\times3} & I \end{bmatrix} \begin{bmatrix} \dot{V}^B \\ \dot{\omega}^B \end{bmatrix} + \begin{bmatrix} \omega^B \times (m\,V^B) \\ \omega^B \times (I\,\omega^B) \end{bmatrix} = \begin{bmatrix} F^B \\ \tau^B \end{bmatrix} \tag{7}$$

The total force acting on the quadrotor includes gravity, gyroscopic effects from rotor spin, and forces/torques from control inputs. These components are structured into a

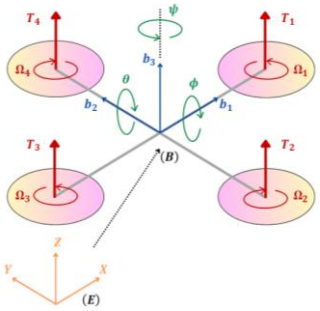

Fig. 1 Schematic of the quadrotor configuration.

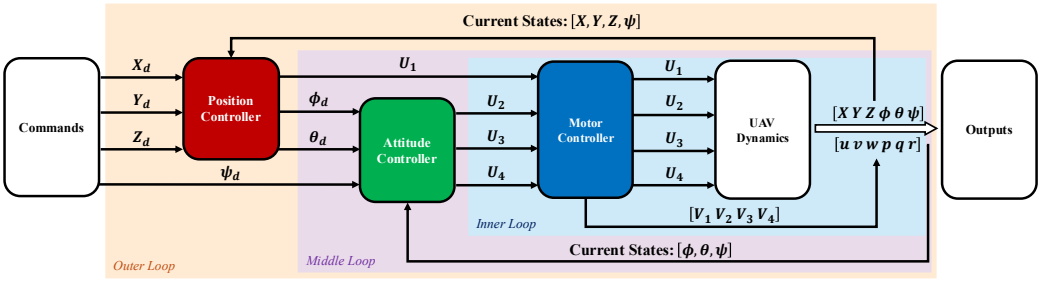

Fig. 2. Developed cascaded hybrid control model.

matrix-form dynamic equation in the B-frame to represent their combined influence:

$$M_B\dot{v} + C_B(v)v = G_B(\xi) + O_B(v)\Omega + E_B\Omega^2 \tag{8}$$

Through the derivation of the above equations, the expressions for the translational and rotational accelerations of the quadrotor for the B-frame can be obtained:

$$\begin{bmatrix} \dot{u} = (vr - wq) + g\sin\theta \\ \dot{v} = (wp - ur) - g\cos\theta\sin\phi \\ \dot{w} = (uq - vp) - g\cos\theta\sin\phi + \dfrac{U_1}{m} \end{bmatrix} \tag{9}$$

$$\begin{bmatrix} \dot{p} = \dfrac{I_{YY} - I_{ZZ}}{I_{XX}}qr - \dfrac{J_{TP}}{I_{XX}}q\Omega + \dfrac{U_2}{I_{XX}} \\ \dot{q} = \dfrac{I_{ZZ} - I_{XX}}{I_{YY}}pr - \dfrac{J_{TP}}{I_{YY}}p\Omega + \dfrac{U_3}{I_{YY}} \\ \dot{r} = \dfrac{I_{XX} - I_{YY}}{I_{ZZ}}pq + \dfrac{U_4}{I_{ZZ}} \end{bmatrix} \tag{10}$$

The control inputs U_1 to U_4 used in the above dynamic equations are nonlinear functions of the individual propeller speeds Ω_1 to Ω_4. These relationships are defined as:

$$\begin{bmatrix} U_1 \\ U_2 \\ U_3 \\ U_4 \end{bmatrix} = \begin{bmatrix} b & b & b & b \\ 0 & -bl & 0 & bl \\ bl & 0 & bl & 0 \\ -d & d & -d & d \end{bmatrix} \begin{bmatrix} \Omega_1^2 \\ \Omega_2^2 \\ \Omega_3^2 \\ \Omega_4^2 \end{bmatrix} \tag{11}$$

These kinematic and dynamic equations form the core of the UAV motion model are all integrated in the UAV dynamics subsystem of the model in Fig. 2. This subsystem is divided into three functional modules: rotor speed mapping, attitude dynamics, and position dynamics. The rotor speed mapping module receives control inputs U_1 to U_4 for calculating the speed of the four electric motors and outputs a total value reflecting the direction of rotation (the corresponding Ω in Eq. (8)). The attitude dynamics module uses these rotational speeds and control inputs U_1 to U_4 to calculate the attitude angles and angular velocities of the quadrotor through Eqs. (6) and (10). The position dynamics module uses the total thrust and the current attitude angle to calculate the acceleration and position change of the quadrotor using Eqs. (5) and (9). These three modules collectively implement a complete 6-DOF flight dynamics.

C. Quadrotor Controller Design

To achieve stable control of the quadrotor under different flight tasks and load conditions, a three-loop cascade hybrid control structure containing position control, attitude control and motor control is constructed, as shown in Fig. 2.

C.1 Position Controller Model

The outer loop position controller is PID control and minimized the positional deviation of the quadrotor in the inertial system through the given desired positional coordinates and outputs the thrust command (U_1) and the desired attitude angles (ϕ_d and θ_d) as inputs to the attitude controller. For the position controller, Eq. (9) needs to be converted to translational equations of motion in E-frame by the rotation matrix (R_Θ):

$$\begin{bmatrix} \ddot{X} = (\sin\psi\sin\phi + \cos\psi\sin\theta\cos\phi)\dfrac{U_1}{m} \\ \ddot{Y} = (-\cos\psi\sin\phi + \sin\psi\sin\theta\cos\phi)\dfrac{U_1}{m} \\ \ddot{Z} = -g + (\cos\theta\cos\phi)\dfrac{U_1}{m} \end{bmatrix} \tag{12}$$

The reference position coordinates are provided by the command module, while the actual position states are obtained from system feedback. The position errors are:

$$\begin{aligned} e_X &= X_{ref} - X \\ e_Y &= Y_{ref} - Y \\ e_Z &= Z_{ref} - Z \end{aligned} \tag{13}$$

To simplify the control design and ensure stable flight and trajectory tracking, the attitude angles roll and pitch (ϕ and θ) are assumed to be very small. The control law of the Z-axis PID controller can be given by the derivation of Eq. (12):

$$U_1 = mg + m\left(k_{p_Z}e_Z + k_{d_Z}\dot{e}_Z + k_{i_Z}\int e_Z dt\right) \tag{14}$$

For the lateral motion in the XY plane, the desired accelerations are calculated form the PID controllers as:

$$\begin{aligned} \ddot{X}_{ref} &= -k_{p_X}e_X - k_{d_X}\dot{e}_X - k_{i_X}\int e_X dt \\ \ddot{Y}_{ref} &= -k_{p_Y}e_Y - k_{d_Y}\dot{e}_Y - k_{i_Y}\int e_Y dt \end{aligned} \tag{15}$$

Thus, the desired roll and pitch angles can be computed based on the translational dynamics:

$$\begin{aligned} \phi_{ref} &= \frac{m}{U_1}\left(-\ddot{X}_{ref}\sin\psi + \ddot{Y}_{ref}\cos\psi\right) \\ \theta_{ref} &= \frac{m}{U_1}\left(\ddot{X}_{ref}\cos\psi + \ddot{Y}_{ref}\sin\psi\right) \end{aligned} \tag{16}$$

Other planning methods like adaptive control, geometrical line-of-sight, or artificial potential fields can reduce sensitivity to these parameters. Nonetheless, this paper primarily aims to propose an integrated energy and control analysis framework for UAVs.

C.2 Attitude Controller Model

The attitude controller receives the desired attitude angles

from the position controller and generates the corresponding control torques (U_2, U_3, U_4) to regulate the roll, pitch and yaw motions of the quadrotor. Since the attitude dynamics are fast, coupled and affected by load disturbances, an MPC is used to achieve accurate tracking. The design of the MPC consists of four key steps including system modeling, state prediction, optimization of control inputs and feedback correction. For the attitude control, Eq. (10) is converted to rotational equations of motion in E-frame by the transfer matrix (T_Θ):

$$\begin{bmatrix} \ddot{\phi} = \frac{I_{YY} - I_{ZZ}}{I_{XX}}\dot{\theta}\dot{\psi} - \frac{J_{TP}}{I_{XX}}\dot{\theta}\Omega + \frac{U_2}{I_{XX}} \\ \ddot{\theta} = \frac{I_{ZZ} - I_{XX}}{I_{YY}}\dot{\phi}\dot{\psi} - \frac{J_{TP}}{I_{YY}}\dot{\phi}\Omega + \frac{U_3}{I_{YY}} \\ \ddot{\psi} = \frac{I_{XX} - I_{YY}}{I_{ZZ}}\dot{\phi}\dot{\theta} + \frac{U_4}{I_{ZZ}} \end{bmatrix} \quad (17)$$

The above rotational equations can be converted to a state space form in continuous time and discretized by the zero-order hold method. Setting the sampling period T to 1 second, the following discrete state space model is obtained:

$$\begin{aligned} x_{k+1} &= A_d x_k + B_d u_k \\ y_k &= C_d x_k \end{aligned} \quad (18)$$

where $x_k \in \mathbb{R}^6$ represents the state vector, $u_k \in \mathbb{R}^3$ is the control input, and $y_k \in \mathbb{R}^3$ is the measured output. A_d, B_d, and C_d are the corresponding system matrices. To improve the response smoothness of the control input, a control incremental variable is introduced as:

$$u_k = u_{k-1} + \Delta u_k \quad (19)$$

Based on this, the augmented state-space equation and output equation are constructed as follow:

$$\begin{aligned} \begin{bmatrix} x_{k+1} \\ u_k \end{bmatrix} &= \begin{bmatrix} A_d & B_d \\ 0 & I \end{bmatrix}\begin{bmatrix} x_k \\ u_{k-1} \end{bmatrix} + \begin{bmatrix} B_d \\ I \end{bmatrix}\Delta u_k \\ y_k &= [C_d \quad 0]\begin{bmatrix} x_k \\ u_{k-1} \end{bmatrix} \end{aligned} \quad (20)$$

During the control process, the controller performs a rolling prediction at each time step over a horizon period of N_p steps. The predicted state and output trajectories are computed recursively based on the augmented system and the current measured state, forming the basis for cost function optimization. To optimize the control input, the following standard quadratic cost function is constructed to penalize output tracking errors and control effort.

$$\mathcal{J} = \frac{1}{2}e_{k+N}^T \bar{S} e_{k+N} + \frac{1}{2}\sum_{i=0}^{N-1} e_{k+i}^T \bar{Q} e_{k+i} + \Delta u_{k+i}^T \bar{R} \Delta u_{k+i} \quad (21)$$

where $e_{k+i} = y_{k+i} - r_{k+i}$ is the output tracking error, and $\bar{S}$, $\bar{Q}$, and $\bar{R}$ are the weighting matrices for the terminal output errors, output tracking errors, and input increments. Instead of applying the entire optimized control sequence, the MPC controller applies only the first control increment Δu_k at each step to update the current state. The controller then re-optimizes the sequence at the next time step based on the latest state. This strategy allows the controller to continuously predict future behavior while incorporating real-time feedback corrections, resulting in more stable, accurate and responsive control performance. In Simulink simulation model, the attitude controller is implemented, and the main controller parameters are listed in Table II. After obtaining the desired angular accelerations ($\ddot{\phi}$, $\ddot{\theta}$, $\ddot{\psi}$) by MPC, the corresponding control torques are computed from the rotational Eq. (17) under the small-angle assumption:

$$U_2 = I_{XX}\ddot{\phi}, \qquad U_3 = I_{YY}\ddot{\theta}, \qquad U_3 = I_{ZZ}\ddot{\psi} \quad (22)$$

TABLE II. MAIN MPC CONTROLLER PARAMETERS

Symbol	Value
Δt	1 s
N_P	80
N_C	15
$\bar{R}$	$\mathrm{diag}(0.1, 0.1, 0.3)$
$\bar{Q}$	$\mathrm{diag}(270, 270, 160)$

C.3 Electric Motor Controller Model

The motor controller is the inner control loop of the quadrotor control architecture. Its main function is to convert the control inputs $U_1 \sim U_4$ from the attitude controller into the reference rotational speeds (ω_i^{ref}) and drive voltages (V_i) required for each motor. These reference rotational speeds are obtained using the thrust allocation formula in Eq. (11).

To simulate the real dynamic response of the voltage input to the motor rotational speed more accurately, the following motor dynamic equation is applied [13]:

$$\dot{\omega}_i = \frac{1}{J_{TP}}\left[-\frac{K_E K_M}{R}\eta N^2 \omega_P - d\omega_P^2 + \frac{K_M}{R}\eta N V_i\right] \quad (23)$$

The actual motor rotational speed ω_i output from the model is fed back and compared to the reference rotational speed. The resulting error is fed into the PID controller and the required voltage to drive the motor is calculated, ensuring accurate speed control.

III. RESULTS AND DISCUSSION

To evaluate the effectiveness and accuracy of the quadrotor dynamic model and the proposed control architecture based on MATLAB and Simulink, it is assumed that the reference tracking task was performed under nominal conditions without external disturbances or sensor noise. In this evaluation, a representative 3D dynamic trajectory was selected as the reference path. The trajectory exhibits a periodic curve in the horizontal plane (X-Y direction) while slowly rising in the Z direction to simulate the flight state of the quadrotor during helical upward flight. The yaw angle (ψ) changes synchronously with time and is used to maintain the continuity of flight orientation. This trajectory setup allows

The 3D trajectory plot in Fig. 3 demonstrates the quadrotor's helical upward flight in space, and the actual flight trajectory is consistent with the reference trajectory. In addition, the actual position of the quadrotor in the X, Y, and Z directions are shown in Fig. 4 in comparison with the reference position, as well as the tracking of the yaw angle. All four plots show that the actual trajectory is highly coincident with the reference trajectory. After verifying the control system, the optimal electric motor specifications for the quadrotor are determined by analyzing the required voltage, power, thrust, and rotational speed during flight. The selection targets a maximum 10-minute flight with full

payload, a total mass of 100 kg, and adherence to the reference trajectory. Additionally, key e-motor parameters to consider are summarized in Table III.

Based on the simulation results shown in Fig. 5(a), although brief spikes in rotational speed are observed during the initial transient phase, these spikes are part of the startup dynamics and do not reflect the steady-state behavior during normal flight. Therefore, the maximum propeller rotational speed after stabilization, approximately 52.27 $rad\ s^{-1}$, is selected as the reference value for motor selection. Considering the gear reduction ratio of $N = 5$, the corresponding motor rotational speed can be calculated as:

$$\omega_{motor} = 5 \times 52.27 = 261.4\ rad\ s^{-1} \approx 2496\ RPM \quad (24)$$

From Figs. 5(b)(c)(d), the following key electric motor requirements during steady flight can be determined. The voltage of each motor is mainly about 55V, and the power

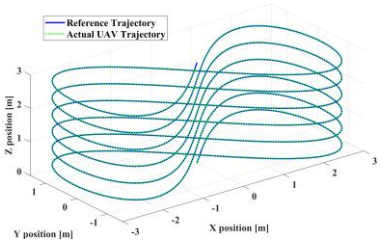

Fig. 3. 3D Helical trajectory tracking.

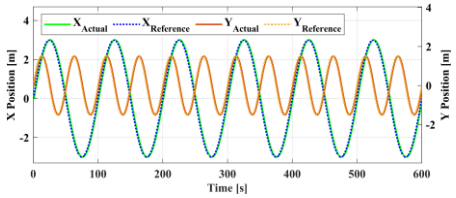

(a)

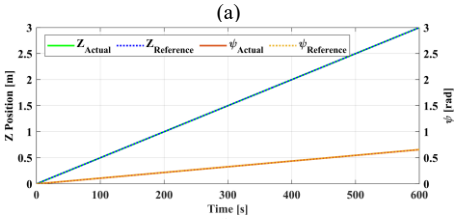

(b)

Fig. 4. The tracking of (a) X- and Y-, and (b) Z-positions, and yaw angle.

TABLE III. MAIN MPC ELECTRICAL MOTOR PARAMETERS

Symbol	Description	Value
M_{motor}	Motor mass	3.9 [kg]
KV	Motor velocity constant	48 [RPM/V]
R	Motor winding resistance	0.5 [Ω]
N	Gear reduction ratio	5
η	Gear transmission efficiency	0.95

consumption is mostly stabilized at approximately 6.2 kW per motor. In terms of thrust, the total output stabilizes around 981.7 N, which means that the thrust demand per rotor is around 245.4 N under stabilized conditions.

A design margin is necessary to ensure safe and robust operation under unforeseen conditions, such as wind disturbances or aggressive maneuvers. Therefore, a 10% performance margin is applied to all key parameters. This requires that each e-motor supports a voltage rating of at least 60.5 V, a continuous power rating of no less than 6.8 kW, and a continuous thrust capacity of approximately 270 N. These values serve as the baseline requirements for selecting the optimal e-motor topology to ensure performance and reliability under full payload flight conditions.

To ensure stable and reliable operation of the quadrotor under full payload conditions, the battery system must be capable of supporting the required voltage, power, and energy demands for the entire flight duration. The selection is guided by the e-motor performance requirements established in the previous section, with consideration of the total flight time, safety margins, and typical characteristics of the battery.

The total energy consumption of the quadrotor over a 10-minute flight is approximately 14.7 MJ (4.1 kWh), as presented in Fig. 5(e). To account for a 10% design margin, the battery must provide at least 16.2 MJ (4.5 kWh) of usable energy. Given that the required voltage of each e-motor is 60.5 V after applying the 10% margin, and all four e-motors are connected in parallel, the battery pack voltage only needs to match the demand of a single e-motor. To meet this requirement, an 18S battery pack configuration (18 cells in series) is suitable, as each LiPo cell typically provides a nominal voltage of 3.7 V and a fully charged voltage of 4.2 V. The resulting nominal battery pack voltage is:

$$\begin{aligned} Nominal\ voltage &= 18 \times 3.7V = 66.6\ V \\ Fully\ charged\ voltage &= 18 \times 4.2V = 75.6\ V \end{aligned} \quad (25)$$

Using the previously established usable energy requirement of 4.5 kWh, the minimum battery capacity is:

$$Capacity = \frac{4.5\ kWh}{60.5\ V} \approx 74.4\ Ah \quad (26)$$

In addition, the battery must support the total continuous power consumption of the quadrotor, which is:

$$Total\ Power = 4 \times 6.8\ kW = 27.2\ kW \quad (27)$$

the battery should sustain a continuous discharge current of:

$$Current = \frac{27.2\ kW}{60.5\ V} \approx 450\ A \quad (28)$$

Since 450A is too much for a single battery, multiple batteries in parallel are considered to share the current load.

To evaluate the performance of the quadrotor under different payload conditions, the payload was simulated by increasing the payload from 0 kg to 50 kg in increments of 5 kg, (total quadrotor mass range of 50 kg to 100 kg). For each case, the key performance indicators, including maximum flight time, energy consumption, e-motor rotational speed and voltage demand need to be obtained. The remaining indicators, except for the maximum flight time, can be obtained directly from the simulation results. The maximum flight time is calculated based on the battery configuration determined in the previous section using:

$$Flight\ Time_{max}\ [min] = \frac{E_{battery}}{P_{total}} \div 60 \quad (29)$$

where $E_{battery}\ [J]$ is the total energy storage of the battery and $P_{total}\ [W]$ is the total power consumption. This provides the maximum flight duration under steady conditions.

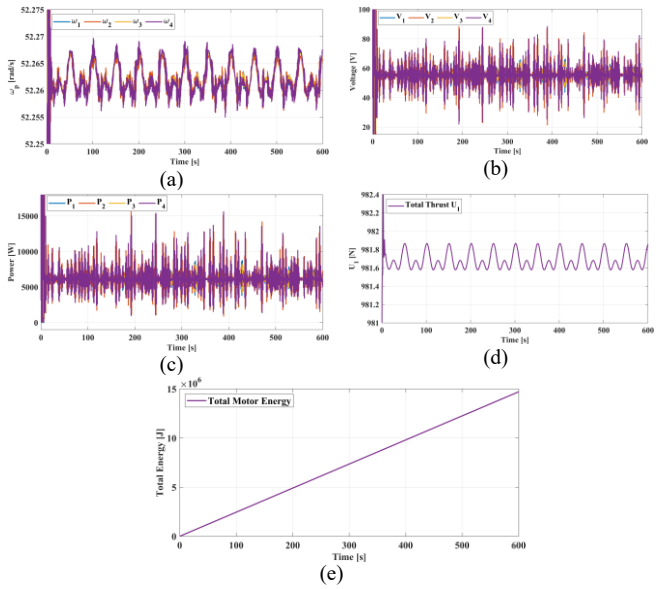

Fig. 5. Electric UAV requirement (a) propeller rotational speed (b) e-motor voltage (c) power (d) total thrust (e) total energy consumption.

The comparison results in Fig. 6 show an approximately linear growth in total energy consumption, e-motor rotational speed, and voltage demand as the payload increases. Specifically, the total energy consumption increases from 7.1 MJ to 14.7 MJ, the e-motor rotational speed increases from 3530 rpm to 4990 rpm, and the voltage demand increases from 38 V to 55 V. The linear increase in voltage and e-motor rotational speed is expected because higher payloads require more thrust to maintain lift, which in turn requires more motor torque and power. In contrast, the maximum flight time calculated with a fixed battery energy of 16.2 MJ decreases as the payload increases from 22.7 minutes at 0 kg to 10.9 minutes at 50 kg, with the rate of decrease slowing down.

Based on our energy sustainability approximations, a typical 10-minute flight consumes 14.7 MJ (≈4.1 kWh), increasing to 16.2 MJ with a 10% power reserve. If powered by the grid, emissions depend on the energy mix. Using Europe's average (0.2 kg CO_2/kWh), a 4.5 kWh emission emits ~1.0 kg CO_2. In contrast, a petrol-powered flight using 1–2 L of fuel emits 3–5 kg CO_2 (2.39 kg CO_2/L). Battery production also has a high carbon cost of ~100 kg CO_2 per 1 kWh. A 4.5 kWh battery pack could generate hundreds of kg of CO_2 during manufacturing. Improving battery efficiency and recycling is essential for sustainable UAV.

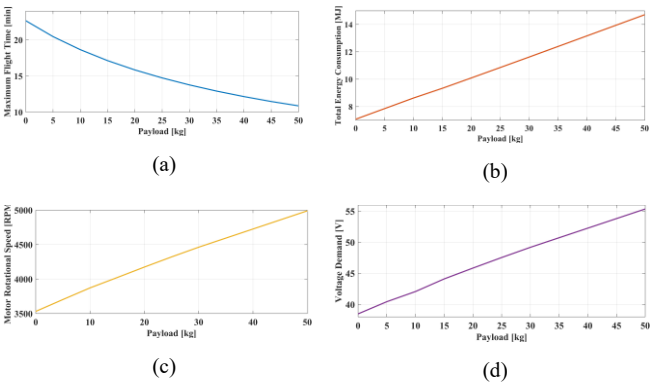

Fig. 5. Performance comparison of (a) flight time, (b) energy consumption, (c) e-motor speed, and (d) e-motor voltage requirement.

IV. Conclusions

An innovative electric propulsion system and its control design analysis framework are presented for the short-range transport requirements of a mid-weight quadrotor electric UAV. By establishing a 6-DOF flight dynamics model and constructing a three-loop cascade control architecture integrating PID and MPC, the system achieves stable trajectory tracking and attitude control in Simulink. The simulation results show that the control strategy is not only able to cope with the strong coupling characteristics and load disturbance during the flight process but also possesses faster dynamic response and stronger steady state accuracy and is able to maintain good flight stability under multiple mission conditions. By analyzing the dynamic response of voltage, speed, power and total thrust during the flight, an optimal electric propulsion system is determined to meet the operation requirements. Each e-motor should provide at least 6.8 kW of power and 270 N of thrust at around 60.5 V. A 10-minute full-payload flight requires at least 4.5 kWh of usable battery energy, with a nominal voltage of about 66.6 V, leading to a minimum capacity of around 67.5 Ah. As payload increases, energy consumption rises linearly, while flight time decreases gradually.

References

[1] A. M. Mazur and R. Domanski, "Hybrid energy systems in unmanned aerial vehicles," Jul. 15, 2019, *Emerald Group Holdings Ltd.* doi: 10.1108/AEAT-08-2018-0218.

[2] J. Zong, B. Zhu, Z. Hou, X. Yang, and J. Zhai, "Evaluation and comparison of hybrid wing vtol uav with four different electric propulsion systems," *Aerospace*, vol. 8, no. 9, Sep. 2021, doi: 10.3390/aerospace8090256.

[3] D. Joshi, D. Deb, and S. M. Muyeen, "Comprehensive Review on Electric Propulsion System of Unmanned Aerial Vehicles," May 14, 2022, *Frontiers Media S.A.* doi: 10.3389/fenrg.2022.752012.

[4] R. Dianovský, P. Pecho, M. Bugaj, and J. Jackuliak, "Economic efficiency comparison of unmanned aerial vehicles with conventional and alternative propulsion systems," in *Transportation Research Procedia*, Elsevier B.V., 2024, pp. 307–317. doi: 10.1016/j.trpro.2024.11.032.

[5] M. Jacewicz, M. Żugaj, R. Głębocki, and P. Bibik, "Quadrotor Model for Energy Consumption Analysis," *Energies (Basel)*, vol. 15, no. 19, Oct. 2022, doi: 10.3390/en15197136.

[6] Y. N. Saravanakumar *et al.*, "Power Sources for Unmanned Aerial Vehicles: A State-of-the Art," Nov. 01, 2023, *Multidisciplinary Digital Publishing Institute (MDPI)*. doi: 10.3390/app132111932.

[7] N. M. Abdulridha, A. Hussien Mary, and A. H. Hisham Jasim, "Optimized PID, FOPID and PIDD 2 for Controlling UAV Based on SSA." [Online]. Available: http://asrjetsjournal.org/.

[8] V. N. Sankaranarayanan, S. Satpute, and G. Nikolakopoulos, "Adaptive Robust Control for Quadrotors with Unknown Time-Varying Delays and Uncertainties in Dynamics," *Drones*, vol. 6, no. 9, Sep. 2022, doi: 10.3390/drones6090220.

[9] I. Lopez-Sanchez and J. Moreno-Valenzuela, "PID control of quadrotor UAVs: A survey," Jan. 01, 2023, *Elsevier Ltd*. doi: 10.1016/j.arcontrol.2023.100900.

[10] B. K. Singh and A. Kumar, "Model predictive control using LPV approach for trajectory tracking of quadrotor UAV with external disturbances," *Aircraft Engineering and Aerospace Technology*, vol. 95, no. 4, pp. 607–618, Feb. 2023, doi: 10.1108/AEAT-12-2021-0368.

[11] A. Patel, A. Banerjee, B. Lindqvist, C. Kanellakis, and G. Nikolakopoulos, "Design and Model Predictive Control of Mars Coaxial Quadrotor," Sep. 2021, doi: 10.1109/AERO53065.2022.9843799.

[12] DJI, "Support for DJI AGRAS T40 - DJI." Accessed: May 04, 2025. [Online]. Available: https://www.dji.com/uk/support/product/t40

[13] T. Bresciani, "Modelling, Identification and Control of a Quadrotor Helicopter," 2008, [Online]. Available: http://www.control.lth.se/publications/.